Short communication

Electrochemical and thermal properties of P2-type $Na_{2/3}Fe_{1/3}Mn_{2/3}O_2$ for Na-ion batteries

Jie Zhao [a], Jing Xu [b], Dae Hoe Lee [b], Nikolay Dimov [c], Ying Shirley Meng [b], Shigeto Okada [c],*

[a] Interdisciplinary Graduate School of Engineering Science, Kyushu University, 6-1, Kasuga Koen, Kasuga 816-8580, Japan
[b] Department of NanoEngineering, University of California San Diego, 9500 Gilman Drive, La Jolla, CA 92093, United States
[c] Institute of Materials Chemistry and Engineering, Kyushu University, 6-1, Kasuga Koen, Kasuga 816-8580, Japan

HIGHLIGHTS

- Single phase P2-type $Na_{2/3}Fe_{1/3}Mn_{2/3}O_2$ was synthesized.
- Both Mn^{3+}/Mn^{4+} and Fe^{3+}/Fe^{4+} take part in the recharge process.
- The material is thermally stable up to ca. 320 °C even in $Na_{0.25}Fe_{1/3}Mn_{2/3}O_2$ state of charge.

ABSTRACT

P2-type $Na_{2/3}Fe_{1/3}Mn_{2/3}O_2$ was prepared by means of solid-state reaction. Its electrochemical properties as a cathode for sodium-ion batteries were investigated in the 1.5—4.3 V range vs. Na metal. This material delivers an initial discharge capacity as high as 193 mAh/g and maintains 153 mAh/g in 40 cycles. Such a high reversible capacity is achieved because both Mn^{3+}/Mn^{4+} and Fe^{3+}/Fe^{4+} become active in the studied voltage range, as confirmed by X-ray absorption spectroscopy (XAS). The thermal stability of charged cathodes was investigated by differential scanning calorimetry (DSC). Although the total heat generated by the fully charged $Na_{0.25}Fe_{1/3}Mn_{2/3}O_2$ is larger than that of the $Li_{0.5}CoO_2$ used as a reference, it is remarkably stable up to ca. 320 °C.

Published by Elsevier B.V.

1. Introduction

Sodium is one of the most abundant elements in the Earth's crust. Therefore sodium is a very attractive charge carrier to replace Li for large stationary applications, where the raw material cost becomes a dominant factor [1,2]. One of the most plausible cathode candidates for sodium-ion batteries is layered rocksalt Na_xMO_2 (M = transition metal). Na_xMO_2 can be categorized into three main groups using the classification proposed by Delmas et al.; the O3, P2, and P3 types [3]. The difference of these structures is whether the alkali atoms occupy octahedral or prismatic sites. So far, various Na_xMO_2 phases, where M represents the first row transition metals V [4,5], Cr [6—8], Fe [9—11], Mn [12—14], Co [15,16], and Ni [17] have

been investigated. Fe and Mn are the most attractive elements for cathodes of large batteries, because of the low environmental impact and cost. O3-type α-NaFeO₂ and α-NaMnO₂ also show electrochemical activity. However, only about 0.4 Na in α-NaFeO₂ and less than 0.8 Na in α-NaMnO₂ could be reversibly extracted, respectively [9,11,12]. Previous studies have revealed that charging α-NaFeO₂ requires formation of high spin Fe^{4+}, yielding unstable structures [13]. Although P2-phase $Na_{0.6}MnO_2$ has an initial capacity of 160 mAh/g [14], the corresponding P2-Na_xFeO_2 does not exist [18]. Related research has shown that different phases can be obtained by various precursors under different synthesis conditions [13,18].

Recently, P2-$Na_{2/3}Fe_{1/2}Mn_{1/2}O_2$ was successfully prepared by Yabuuchi et al. This phase has an initial capacity of 190 mAh/g and still delivered 150 mAh/g after 30 full recharge cycles [18]. We have expanded this study and prepared P2-$Na_{2/3}Fe_{1/3}Mn_{2/3}O_2$. To the best of our knowledge, P2-$Na_{2/3}FeO_2$ cannot be synthesized and

Mn is used as a P2-phase promoter and stabilizer. In general, the more stable Na-ion host, the better rechargeable capacity. Larger Mn content is therefore likely to result in a more stable cycle life, which is one of the objectives in this work. Mortemard de Boisse et al. successfully obtained P2–$Na_{2/3}Fe_{1/3}Mn_{2/3}O_2$ by auto-combustion synthesis from $Fe(NO_3)_3$, $NaNO_3$ and glycine [13]. The capacity fading of the sample thus prepared was somewhat faster than that of P2–$Na_{2/3}Fe_{1/2}Mn_{1/2}O_2$ obtained from Na_2O_2, Fe_2O_3 and Mn_2O_3 in a study by Yabuuchi et al. [18]. This result is contrary to the general expectation that the larger Mn content in the P2–$Na_{2/3}Fe_xMn_{1-x}O_2$ phase would actually stabilize the structure. In our opinion, the auto-combustion synthesis method and precursors may have a striking impact on the properties of the samples [19–21].

In this paper, we synthesized $Na_{2/3}Fe_{1/3}Mn_{2/3}O_2$ from Na_2O_2, Fe_2O_3 and Mn_2O_3 precursors to check our hypothesis. The P2-structure of the material was confirmed by means of X-ray diffraction (XRD), the charge compensation mechanisms were identified using X-ray absorption spectroscopy (XAS), and the thermal stability was evaluated by differential scanning calorimetry (DSC).

2. Experimental

A solid-state reaction was utilized to synthesize the compounds. 97% Na_2O_2 (Wako Pure Chemical Industries, Ltd.), 99.7% Fe_2O_3 and 98% Mn_2O_3 (Sigma–Aldrich Co. LLC.) were used as precursors. Na_2O_2 serves not only as a source of Na, but also as an oxidizer that helps in obtaining a single-phase pure material [13]. Stoichiometric amounts of Na–Fe–Mn precursors were mixed in an Ar-filled glove box and pelletized. The pellets were calcined at 900 °C for 12 h in air and quenched to room temperature by removing the samples from the furnace. The samples were stored in an Ar-filled glove box.

Cathodes were prepared by mixing 80 wt% active material with 10 wt% acetylene black, and then the powders were mixed with an appropriate amount of 5 wt% PVDF solution in NMP. The slurry was pasted on an Al current collector and dried under a vacuum at 80 °C. After drying, circular electrodes were punched in circular with 15-mm diameter and dried again overnight at 120 °C in a vacuum oven.

The separator was a porous polypropylene film (Celgard 3501) and sodium metal foil was used as a counter electrode. A 1 M $NaPF_6$ in propylene carbonate (PC) solution was used as the electrolyte. The coin-type cells were assembled in an Ar-filled glove box with a dew point below −80 °C, to prevent the oxidation of Na anode. Galvanostatic cycling tests were conducted between 1.5 V and 4.3 V at a rate of 12 mA g^{-1}.

The powder X-ray diffraction (XRD) measurements were performed using a Bruker D8 advance diffractometer with a Bragg–Brentano θ–2θ geometry and a Cu Kα source (λ = 1.54 Å). Samples were scanned from 10° to 70° with a scan rate of 0.025° per second. XRD data analysis was carried out by means of Rietveld refinement using the FullProf software package [22].

The morphologies were examined with a scanning electron microscope (SEM, Philips, XL30) at an accelerating voltage of 20 kV.

X-ray absorption spectroscopy (XAS) was carried out at beamline 20-BM of the Advanced Photon Source (APS) at Argonne National Laboratory (ANL). The electrode samples were obtained by disassembling the batteries in the Ar-filled glove box and then washed 3 times using battery grade diethyl carbonate (DEC). Transmission spectra at the Mn K-edge (6539 eV) and Fe K-edge (7112 eV) were collected along with a simultaneous spectrum on a reference foil of metallic Mn and Fe to assure consistent energy calibration. Energy calibration was carried out by using the first

derivative in the spectra of Fe and Mn metal foils. Data were analyzed and refined using the Ifeffit [23] and Horae [24] packages.

TG-DSC (Thermo plus TG-DSC8230, Rigaku) experiments were carried out using cathode pellets on predefined states of charge obtained during the first charging. Test electrode pellets contained 80 wt% $Na_{2/3}Fe_{1/2}Mn_{2/3}O_2$, 10 wt% acetylene black, and 10 wt% polytetrafluoroethylene (PTFE, Daikin Industries, Ltd.). After reaching a certain predefined state of charge, the test cells were disassembled in the Ar-filled glove box, rinsed and soaked in DMC for 4 h. Then the electrodes were vacuum-dried at room temperature for 12 h, to remove DMC absorbed during the rinsing step. The washed and dried cathode pellet sample was sealed into a stainless-steel pan. The pan was heated from room temperature to 500 °C at a rate of 5 °C/min. During the entire temperature sweep, the TG signal was monitored simultaneously to confirm the tightness of the hermetically sealed pan.

3. Results and discussion

The Rietveld refinement of the XRD pattern of the as-synthesized P2–$Na_{2/3}Fe_{1/3}Mn_{2/3}O_2$ is shown in Fig. 1. The refined lattice parameters were a = 2.913 Å and c = 11.269 Å. The refinement was performed in the $P63/mmc$ space group and the R-factors were R_{wp} = 2.00 and R_B = 10.20, as shown in Table 1. All the peaks are sharp and well defined, indicating that the crystallinity of the compound is high. The refinement is in a good agreement with the P2-single phase without any impurities. Particle morphology was observed by SEM. The primary particle size was distributed between 500 nm and 2 μm and the particles were agglomerated to each other, forming several micrometer sized secondary particles. The particle size and particle size distribution of our material were in good agreement with the previous reports [13,18].
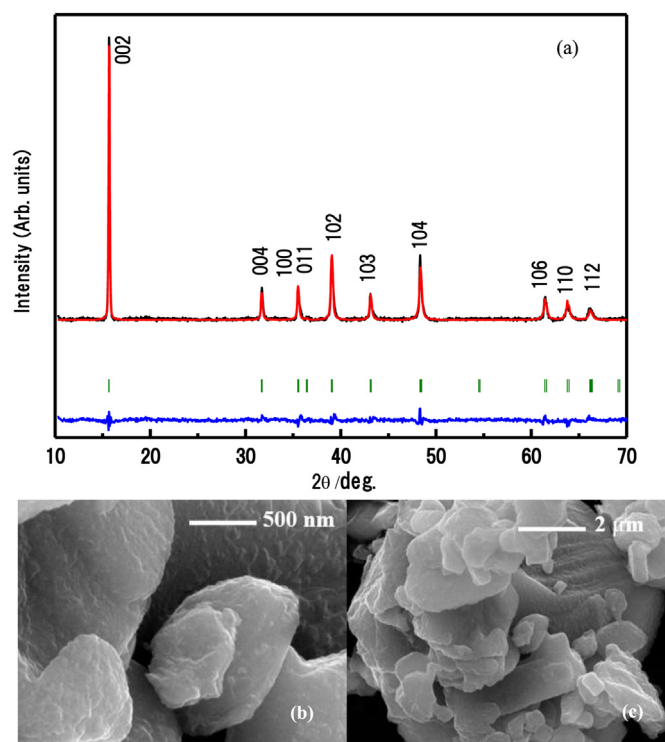
Fig. 1. (a) XRD pattern of P2-type $Na_{2/3}Fe_{1/3}Mn_{2/3}O_2$. The structure refinement was carried out by the Rietveld method using the FullProf software package. Particle morphology was observed by SEM at different magnifications, (b) 50000× and (c) 12500×.

Table 1
Parameters and reliability factors deduced from the Rietveld refinement data for P2−Na$_{2/3}$Fe$_{1/3}$Mn$_{2/3}$O$_2$.

Space group: $P6_3/mmc$					
$a = b = 2.913$ Å, $c = 11.269$ Å,					
$R_{wp} = 2.00$, $R_B = 10.20$					
Atom	Site	x	y	z	Occ.
Fe	2a	0	0	0	1/3
Mn	2a	0	0	0	2/3
O	4f	1/3	2/3	0.09	2.00
Na$_f$	2b	0	0	0.25	0.26
Na$_e$	2d	1/3	2/3	0.75	0.43

The voltage profiles and the cyclability of Na$_{2/3}$Fe$_{1/3}$Mn$_{2/3}$O$_2$ in 1 M NaPF$_6$ PC electrolyte between 1.5 V and 4.3 V at C/20 rate vs. Na$^+$/Na are shown in Fig. 2. The fully charged state of Na$_{2/3}$Fe$_{1/3}$Mn$_{2/3}$O$_2$ corresponds to Na$_{0.2}$Fe$_{1/3}$Mn$_{2/3}$O$_2$, while the fully discharged one is NaFe$_{1/3}$Mn$_{2/3}$O$_2$. Two distinctive slope and plateau regions are observed during the first charge. Higher Mn content brought a longer slope region due to the Mn^{3+}/Mn^{4+} redox couple. On the other hand, the Fe^{3+}/Fe^{4+} redox couple seems to become active at the plateau region above 4.1 V. The second charge/discharge capacities were around 204 mAh/g and 191 mAh/g, respectively. After 40 cycles, the discharge capacity was still 153 mAh/g. Therefore, the P2−Na$_{2/3}$Fe$_{1/3}$Mn$_{2/3}$O$_2$ material showed a similar high reversible capacity and better cycle life than the previously reported P2−Na$_{2/3}$Fe$_{1/2}$Mn$_{1/2}$O$_2$ [18]. It is noteworthy that we could obtain the good performance without any electrolyte additives such as fluoroethylenecarbonate (FEC) or vinyl-idenecarbonate (VC). Mortemard de Boisse et al. have explained the fast capacity fading of P2−Na$_x$Mn$_{1−y}$Fe$_y$O$_2$ phases due to electrolyte decomposition, which in their case proceeded even at 3.8 V. We charged our P2−Na$_{2/3}$Fe$_{1/3}$Mn$_{2/3}$O$_2$ cathode pellets to 4.3 V against Na. Nevertheless we could observe a better cyclability. Therefore, the electrolyte decomposition alone is not sufficient to explain the degradation behavior of these materials. One speculation is that our experimental conditions (Na$_2$O$_2$ + Mn$_2$O$_3$ + Fe$_2$O$_3$ precursors) yield material with better structural integrity. Further study will be necessary to compare the stability of these materials obtained by different synthetic routes.

The Fe K-edge (7112 eV) and Mn K-edge (6539 eV) X-ray absorption near-edge structure (XANES) spectra of pristine and cycled samples are shown in Fig. 3. When the cathode was charged to 4.1 V (Fig. 3a), the Fe K-edge spectrum shifted slightly compared with the as-prepared state. However, a much more clear shift towards the higher energy region was observed in the Mn K-edge spectrum (Fig. 3b). This indicates that the oxidization of Mn-ions mainly compensates for the electron loss at this step. When the material was further charged to 4.3 V, the shift to the higher energy region in the Fe K-edge was clearly seen. On the other hand, no obvious change was shown in the Mn K-edge. Similar phenomena have been reported for the P2−Na$_{2/3}$Fe$_{1/2}$Mn$_{1/2}$O$_2$ compound [18], demonstrating that Fe^{4+} is also activated in P2−Na$_{2/3}$Fe$_{1/3}$Mn$_{2/3}$O$_2$ at the high voltage range. After P2−Na$_{2/3}$Fe$_{1/3}$Mn$_{2/3}$O$_2$ was discharged to 2.0 V, the Fe K-edge basically returned to the same position with the as-prepared state, suggesting good reversibility in its electronic structure change. In addition, the Mn K-edge moved to a lower energy region compared with the as-prepared state. This is consistent with the observed electrochemical result; more Na-ions than in the original stoichiometry are inserted into the electrode after it is discharged to 2.0 V, leading to a reduction of more Mn-ions and thus lower energy for the Mn K-edge. Based on the XANES spectra for the Fe and Mn K-edges, it was demonstrated that Mn^{3+}/Mn^{4+} is the

Fig. 2. Voltage profiles and the cyclability of Na$_{2/3}$Fe$_{1/3}$Mn$_{2/3}$O$_2$ at a rate of 12 mA/g in the voltage range of 1.5 V and 4.3 V.
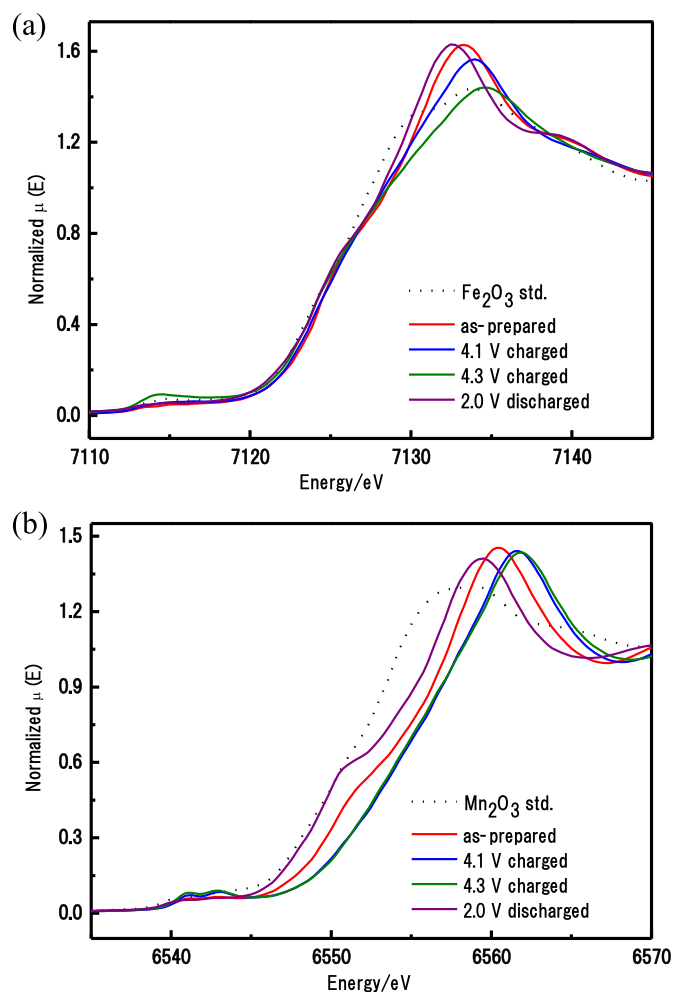
Fig. 3. (a) Fe K-edge and (b) Mn K-edge XAS analysis of Na$_{2/3}$Fe$_{1/3}$Mn$_{2/3}$O$_2$ charged to 4.3 V and discharged to 2.0 V.

major redox couple when the voltage is below 4.1 V, and Fe^{4+} begins to be activated at the higher voltage region.

As the thermal stabilities of any new electrode active material candidates are important, the thermal stability of $Na_{2/3}Fe_{1/3}Mn_{2/3}O_2$ under various states of charge must be systematically evaluated. A standard figure of merit for the thermal stability of a given electrode material is the enthalpy liberated in the course of temperature sweep, which can be conveniently measured by means of TG-DSC. Charging of $Na_{2/3}Fe_{1/3}Mn_{2/3}O_2$ corresponds to sodium removal yielding $Na_xFe_{1/3}Mn_{2/3}O_2$ phases with $x < 2/3$. Mn^{3+}/Mn^{4+} is the main active redox couple when the voltage is below 4.1 V, and Fe^{3+} begins to be oxidized above 4.1 V. It is concerned that the presence of the unstable high-spin Fe^{4+} in the crystal lattice above 4.1 V will reduce the thermal stability of the charged compound. Fig. 4 shows DSC curves of $Na_xFe_{1/3}Mn_{2/3}O_2$ charged to 4.0 V ($x = 0.46$), 4.2 V ($x = 0.36$), and 4.3 V ($x = 0.25$), respectively. The interested exothermic peaks were clearly detected between 330 °C and 460 °C. Deeper charging clearly brings larger heat generation, because the lower sodium content in the $Na_xFe_{1/3}Mn_{2/3}O_2$ structure increases its oxidation power. The exothermic peaks must be the oxidation of AB by $Na_xFe_{1/3}Mn_{2/3}O_2$ in the hermetically sealed pan.

The electrodes charged to 4.2 V and 4.3 V showed, clearly split large exothermic peaks around 446 °C and 438 °C. On the other hand, charging to 4.0 V resulted in a very broad peak around 400 °C with the released total energy being less than half of than at 4.3 V charged state. We speculate that the TG-DSC peak splitting at the higher states of charge is due to the presence of both Mn^{4+} and Fe^{4+} above 4.0 V. Charging to 4.3 V results in $Na_{1/4}Fe_{1/3}Mn_{2/3}O_2$, which releases 645 J/g. This is a 2.5 times larger exothermic heat than that of fully charged $Li_{0.5}CoO_2$. While the exothermic reactions of charged $Na_xFe_{1/3}Mn_{2/3}O_2$ appeared above 330 °C, $Li_{0.5}CoO_2$ showed the sharp exothermic peak below 200 °C, corresponding to the phase transition [25].

Another important feature of the DSC curve, which has been largely overlooked, is the rate of heat generation dQ/dt. There are at least two ways to quantify this parameter. The width of the DSC peak gives a reasonable estimate for the speed of the reaction. However, we believe that a more precise quantity that would more correctly represent the conditions favoring the thermal runaway of any charged cathode would be the derivative of the heat flow dQ/dt [mW/(mgs)]. This is because even smaller amounts of heat flow, when released instantly, are more likely to give rise to thermal

runaway than larger heat flow that is released slowly, which would allow dissipation in the ambient environment. Estimated values of dQ/dt are shown in Fig. 4. Even the $Na_xFe_{1/3}Mn_{2/3}O_2$ sample charged to 4.3 V shows smaller dQ/dt than $Li_{0.5}CoO_2$ used as a reference. $Na_xFe_{1/3}Mn_{2/3}O_2$ samples charged to 4.0 V and 4.2 V lead to very broad exothermic peaks with dQ/dt values less than half that of the $Li_{0.5}CoO_2$ standard.

4. Conclusions

In order to improve the stability of P2 phase, Mn rich $Na_{2/3}Fe_{1/3}Mn_{2/3}O_2$ was synthesized by means of a solid-state reaction using Na_2O_2, Fe_2O_3, and Mn_2O_3 precursors. The second discharge capacity was around 191 mAh/g, and a 153 mAh/g discharge capacity was still delivered after 40 cycles between 1.5 V and 4.3 V in the conventional $NaPF_6$ electrolyte without any additives. Similar to P2–$Na_{2/3}Fe_{1/2}Mn_{1/2}O_2$, the existence of Mn^{4+} and Fe^{4+} were clearly confirmed in the charged state by XAS. Further improvement of these materials should be possible by doping other transition metals such as Ni [26].

Electrochemically desodiated $Na_xFe_{1/3}Mn_{2/3}O_2$ ($x = 0.46$, 0.36 and 0.25) showed clear exothermic peaks between 330 °C and 460 °C. Charging to 4.3 V results in $Na_{1/4}Fe_{1/3}Mn_{2/3}O_2$, which releases 645 J/g. This total heat release was larger than that of $Li_{0.5}CoO_2$, which was used as a reference. However, the heat release in this case evolved slowly between 330 °C and 460 °C, while $Li_{0.5}CoO_2$ decomposed completely in the narrow temperature range between 350 °C and 420 °C. Moreover, even in its fully charged state $Na_{1/4}Fe_{1/3}Mn_{2/3}O_2$ does not release heat below 330 °C. In contrast, $Li_{0.5}CoO_2$ is known to undergo an exothermic phase transition from layered rocksalt to spinel structure around 190 °C. Therefore, these materials could be a viable alternative to their lithium-ion counterparts.

References

[1] M.D. Slater, D. Kim, E. Lee, C.S. Johnson, Adv. Funct. Mater. 23 (2013) 947.
[2] H. Pan, Y.S. Hu, L. Chen, Energy Environ. Sci. 6 (2013) 2338.
[3] C. Delmas, C. Fouassier, P. Hagenmuller, Phys. B+C 99 (1980) 81.
[4] C. Didier, M. Guignard, C. Denage, O. Szajwaj, S. Ito, I. Saadoune, J. Darriet, C. Delmas, Electrochem. Solid-State Lett. 14 (5) (2011) A75.
[5] D. Hamani, M. Ati, J.-M. Tarascon, P. Rozier, Electrochem. Commun. 13 (2011) 938.
[6] J.-J. Ding, Y.-N. Zhou, Q. Sun, Z.-W. Fu, Electrochem. Commun. 22 (2012) 85.
[7] X. Xia, J.R. Dahn, Electrochem. Solid-State Lett. 15 (1) (2012) A1.
[8] C.-Y. Chen, K. Matsumoto, T. Nohira, R. Hagiwara, A. Fukunaga, S. Sakai, K. Nitta, S. Inazawa, J. Power Sources 237 (2013) 52.
[9] J. Zhao, L. Zhao, N. Dimov, S. Okada, T. Nishida, J. Electrochem. Soc. 60 (2013) A3077.
[10] N. Yabuuchi, H. Yoshida, S. Komaba, Electrochem. Commun. 80 (10) (2012) 716.
[11] Y. Takeda, K. Nakahara, M. Nishijima, N. Imanishi, O. Yamamoto, M. Takano, R. Kanno, Mat. Res. Bull. 29 (1994) 659.
[12] X.H. Ma, H.L. Chen, G. Ceder, J. Electrochem. Soc. 158 (2011) A1307.
[13] B. Mortemard de Boisse, D. Carlier, M. Guignard, C. Delmas, J. Electrochem. Soc. 160 (4) (2013) A569.
[14] A. Caballero, L. Hernán, J. Morales, L. Sánchez, J. Santos Peña, M.A.G. Aranda, J. Mater. Chem. 12 (2002) 1142.
[15] C. Delmas, J.J. Braconnier, C. Fouassier, P. Hagenmuller, Solid State Ionics 3/4 (1981) 165.
[16] R. Berthelot, D. Carlier, C. Delmas, Nat. Mater. 10 (2011) 74.
[17] P. Vassilaras, X.H. Ma, X. Li, G. Ceder, J. Electrochem. Soc. 160 (2) (2013) A207.
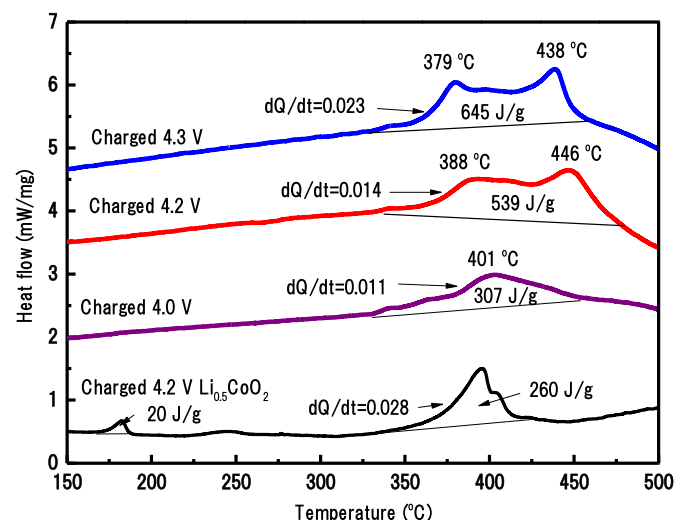
Fig. 4. DSC curves of $Na_xFe_{1/3}Mn_{2/3}O_2$ charged to 4.0 V, 4.2 V, or 4.3 V, respectively. The samples were heated from room temperature to 500 °C at a rate of 5 °C/min.

[18] N. Yabuuchi, M. Kajiyama, J. Iwatate, H. Nishikawa, S. Hitomi, R. Okuyama, R. Usui, Y. Yamada, S. Komaba, Nat. Mater. 11 (2012) 512.
[19] Y. Xia, H. Takeshige, H. Noguchi, M. Yoshio, J. Power Sources 56 (1995) 61.
[20] N. Yabuuchi, T. Ohzuku, J. Power Sources 119 (2003) 171.
[21] C.R. Brown, E. McCalla, J.R. Dahn, Solid State Ionics 253 (2013) 234.
[22] J. Rodriguez-Carvajal, Phys. B 192 (1993) 55.
[23] M. Newville, J. Synchrotron Radiat. 8 (2001) 322.
[24] B. Ravel, M. Newville, J. Synchrotron Radiat. 12 (2005) 537.
[25] Y. Baba, S. Okada, J. Yamaki, Solid State Ionics 148 (2002) 311.
[26] D. Yuan, X. Hu, J. Qian, F. Pei, F. Wu, R. Mao, X. Ai, H. Yang, Y. Cao, Electrochim. Acta 116 (2014) 300.